



This is a repository copy of *Controlling the composition and position of metal–organic frameworks via reactive inkjet printing*.

White Rose Research Online URL for this paper:

<https://eprints.whiterose.ac.uk/197719/>

Version: Published Version

---

**Article:**

Gregory, D.A. [orcid.org/0000-0003-2489-5462](https://orcid.org/0000-0003-2489-5462), Nicks, J., Artigas-Arnaldas, J. et al. (3 more authors) (2023) Controlling the composition and position of metal–organic frameworks via reactive inkjet printing. *Advanced Materials Interfaces*, 10 (12). 2300027. ISSN 2196-7350

<https://doi.org/10.1002/admi.202300027>

---

**Reuse**

This article is distributed under the terms of the Creative Commons Attribution (CC BY) licence. This licence allows you to distribute, remix, tweak, and build upon the work, even commercially, as long as you credit the authors for the original work. More information and the full terms of the licence here:

<https://creativecommons.org/licenses/>

**Takedown**

If you consider content in White Rose Research Online to be in breach of UK law, please notify us by emailing [eprints@whiterose.ac.uk](mailto:eprints@whiterose.ac.uk) including the URL of the record and the reason for the withdrawal request.



[eprints@whiterose.ac.uk](mailto:eprints@whiterose.ac.uk)  
<https://eprints.whiterose.ac.uk/>

# Controlling the Composition and Position of Metal–Organic Frameworks via Reactive Inkjet Printing

David Alexander Gregory, Joshua Nicks, Joaquin Artigas-Arnaudas, Michael S. Harris, Jonathan A. Foster,\* and Patrick J. Smith\*

Reactive inkjet printing (RIJ) is demonstrated as a new approach to the patterning of surfaces with metal–organic frameworks (MOFs). RIJ is an emerging manufacturing technique that jets solutions of reagents onto a substrate allowing them to react in situ to form the desired material. MOFs have the potential to perform a variety of useful sensing, catalytic, separation and storage applications within sophisticated devices, however, their insolubility makes them challenging to process into complex shapes and patterns. The RIJ approach offers advantages over conventional inkjet printing in that it allows stable solutions of different ligand and metal ions to be combined in a “mix-and-match” way. Here, the benefits of the RIJ approach are demonstrated to optimize the stoichiometry of the printed MOF, print a variety of different frameworks using common inks, and create gradients where the composition of the printed MOFs gradually varies between one isorecticular structure and another. Proof of principle is also demonstrated for the approach by demonstrating size selective encapsulation of a dye within a RIJ printed MOF. It is anticipated that this approach will be broadly applicable to the printing of MOFs and related materials enhancing their use across a variety of different applications.

## 1. Introduction

Metal–organic frameworks (MOFs) are a diverse class of materials formed by reacting organic ligands with metal-ions to form crystalline co-ordination compounds consisting of porous networks. The high internal surface areas and readily tuneable chemistry of MOFs mean they have found use in a wide variety of applications,<sup>[1]</sup> including: gas-storage and separation,<sup>[2]</sup> catalysis,<sup>[3]</sup> sensing,<sup>[4]</sup> water-purification,<sup>[5]</sup> drug release,<sup>[6]</sup> and electronics.<sup>[7]</sup> However, the insolubility of MOFs makes it challenging to process them into the often complex shapes and patterns required for real world applications which limits their use in sophisticated devices.<sup>[8]</sup> As such, a diverse range of approaches have been explored for growing, depositing and patterning MOFs onto surfaces.<sup>[9]</sup> These include: spray coating,<sup>[10]</sup> spin coating,<sup>[11]</sup> dip-coating,<sup>[11,12]</sup> soft lithography,<sup>[13]</sup> microfluidic<sup>[14]</sup> and 3D printing,<sup>[15]</sup> electrospinning,<sup>[16]</sup> and gel monolith approaches.<sup>[15c,17]</sup>


Inkjet printing is a widely used approach for depositing complex patterns onto surfaces and offers a variety of advantages including minimal wastage, large-area depositions and integration with computer-aided design (CAD) information.<sup>[18]</sup> Flexible displays,<sup>[19]</sup> solar cells,<sup>[20]</sup> catalysts,<sup>[21]</sup> explosive sensors,<sup>[22]</sup> transistors,<sup>[23]</sup> data<sup>[24]</sup> and energy storage devices<sup>[25]</sup> as well as, biological materials<sup>[26]</sup> and medical devices<sup>[27]</sup> have all been produced through inkjet printing of a variety of different organic and inorganic functional materials. In particular, several examples of inkjet printed MOFs have been reported and employed for sensing,<sup>[28]</sup> anti-counterfeiting,<sup>[29]</sup> security,<sup>[30]</sup> and electrocatalysis<sup>[31]</sup> applications.

Two distinct approaches have so far been developed to enable the inkjet printing of MOFs. The first, pioneered by Zhuang et al.<sup>[32]</sup> used a single MOF precursor solution containing both ligands and metal-ions as an ink which they were able to print using a commercial inkjet printer onto a variety of substrates. Similar approaches have been used to synthesize several other MOFs,<sup>[28,30]</sup> however samples required repeated drying and washing cycles to build up layers and remove high boiling point solvents. The second approach was developed by

D. A. Gregory  
 Department of Materials Science and Engineering  
 University of Sheffield  
 Sheffield S1 3JD, UK

J. Nicks, M. S. Harris, J. A. Foster  
 Department of Chemistry  
 University of Sheffield  
 Brook Hill, Sheffield S3 7HF, UK  
 E-mail: jona.foster@sheffield.ac.uk

J. Artigas-Arnaudas, P. J. Smith  
 Department of Mechanical Engineering  
 University of Sheffield  
 Garden Street, Sheffield S1 4BA, UK  
 E-mail: patrick.smith@sheffield.ac.uk

 The ORCID identification number(s) for the author(s) of this article can be found under <https://doi.org/10.1002/admi.202300027>.

© 2023 The Authors. Advanced Materials Interfaces published by Wiley-VCH GmbH. This is an open access article under the terms of the Creative Commons Attribution License, which permits use, distribution and reproduction in any medium, provided the original work is properly cited.

DOI: 10.1002/admi.202300027

Luz et al.<sup>[29]</sup> who printed aqueous inks consisting of a suspension of pre-formed nanoparticles of three different lanthanide MOFs along with ethanol as an anti-solvent to accelerate precipitation. A similar approach has been used by Su et al.<sup>[31]</sup> to print porphyrinic MOFs. Both sets of authors discuss the challenges associated with this approach in creating stable suspensions which can otherwise clog print-heads. A possible third approach was pioneered by Hou et al.<sup>[33]</sup> by directly synthesizing an enzyme-MOF composite. MOF precursors and proteins were loaded into different cartridges of a desktop color printer and the composites were generated in pre-determined patterns on the surface of various substrates such as paper and polymeric films.

Reactive inkjet printing (RIJ) is an additive manufacturing technique which generates materials on the substrate, at the point of interest. RIJ can avoid some of the challenges associated with creating suspensions/inks such as stability, life-time and nozzle-clogging, and so broaden the pallet of materials that can be printed.<sup>[18,26a,b,34]</sup> In RIJ, separate stable solutions of two or more reactants are printed in the same location and react on the surface to produce the desired material *in situ*. RIJ enables precise control of picolitre size droplets which improves mixing and heat transfer making the reaction more efficient and the overall process consume less material. RIJ can also improve process safety in some applications, as demonstrated by Lennon *et al.*<sup>[34]</sup> who created patterned layers of SiO<sub>2</sub> by direct etching of hydrofluoric acid, which was synthesized *in situ*, and at point of use, via RIJ. Additionally, the use of an inkjet printer allows for the reactant stoichiometry, synthesis conditions and composition to be readily varied during printing which is not possible with pre-mixed solutions.<sup>[18a]</sup> One of the first examples of RIJ being used to produce gradients was demonstrated by Jabbour *et al.* who were able to vary the sheet resistance of a conducting polymer by selectively printing an oxidant.<sup>[18b]</sup>

Here we demonstrate the use of RIJ as a precise approach for the synthesis and patterning of MOFs onto substrates and for creating gradients where the structure of one MOF controllably and gradually transforms into a second MOF. Separate inks consisting of either ligands, or metal-ions, dissolved in DMF are deposited simultaneously onto a substrate, where they react resulting in MOF formation. Wagner, Richardson *et al.*<sup>[35]</sup> recently reported reactive extrusion printing as a related approach in which syringes full of different reagents are combined through touching needles to print HKUST-1. In this work we use a custom-built printhead and system to print picolitre droplet size allows efficient mixing and rapid evaporation of the solvent results in well-defined patterns. We demonstrate the synthesis of a range of MOF architectures which have found applications in adsorption and separation, catalysis, sensing, as well as optical and electronic applications.<sup>[36]</sup> Furthermore, by not using pre-formed MOF crystallites the RIJ technique allows for the patterning of surfaces with gradients of MOFs with different ratios of building blocks. As a step toward these type of lab-on-a-chip applications, we demonstrate that printed MOFs retain their well-defined pores and can therefore be used to selectively encapsulate specific dyes whilst rejecting others.

## 2. Results and Discussion

### 2.1. RIJ of Cu<sub>3</sub>(BTC)<sub>2</sub>

Inks were formed by separately dissolving the respective metal acetate salt and ligand in dimethylformamide (DMF) as 0.25 molar solutions of each. Acetate salts, rather than the more commonly used nitrate salts, were chosen as they are known to accelerate the synthesis of paddlewheel-based MOFs by performing the desired secondary building unit. DMF was selected as its high boiling point and the ability to dissolve both the organic ligands and metal salts in the same solvent made it attractive for this first study. The rheological properties of the solutions were measured in order to investigate the “jet-ability” of the inks (ESI Table 1), with both being observed to jet stably (Figure 1).

RIJ of the MOFs was achieved using a custom-built inkjet printer, based on the JetLab system (MicroFab, Plano, and TX) fitted with an angled jetting device assembly as depicted in Figure 1. The set-up was designed to allow the simultaneous printing of two inks onto the same location of the substrate.

The sample stage was adjusted to ensure that the droplets touched the surface at exactly the intercept point leading to the formation of clearly defined droplets. Initial studies focused on the formation of the archetypal MOF popularly known as HKUST-1,<sup>[37]</sup> which has the structure Cu<sub>3</sub>(BTC)<sub>2</sub>(DMF)<sub>3</sub>, where BTC is 1,3,5-benzenetricarboxylate. Strobe time lapse images were taken (Figure 1) of the ligand, H<sub>3</sub>BTC, and metal salt, Cu(OAc)<sub>2</sub> during the printing of the Cu<sub>3</sub>(BTC)<sub>2</sub> lines. The copper acetate ink was observed to result in slightly smaller droplets than the H<sub>3</sub>BTC ink (Figure 1). The small ink volume (2–10 pL) allows for fast drying of the ink solvent and samples appeared dry after ≈10–30 s, the exact duration being dependent on the deposited droplet amount.

Based on the stoichiometry of Cu<sub>3</sub>(BTC)<sub>2</sub>(DMF)<sub>3</sub>, a 2:3 ratio of ligand:metal solutions was expected to be optimal. However, it is worth noting that Terfort and co-workers used an excess of metal-ions (1:2 ratio) to print Cu<sub>3</sub>(BTC)<sub>2</sub>.<sup>[32]</sup> In our work, we used RIJ to deposit both components, H<sub>3</sub>BTC and Cu(OAc)<sub>2</sub>, at different ratios (1:1, 1:2, 1:3, 2:3, 3:2, 3:1, and 2:1) to optimize stoichiometry. Successive droplets were jetted at a frequency of 25 Hz. As an example, a dot array with a ratio of 1:3 was achieved by simultaneously jetting one drop of H<sub>3</sub>BTC and one of Cu(OAc)<sub>2</sub> followed by two additional drops of Cu(OAc)<sub>2</sub> at 25 Hz. In order to improve signal to noise ratios for the various analysis techniques this process was repeated five times at each location (to increase the amount of deposited material) before moving to the next.

RIJ of samples with the 2:3 ratio, which was expected to result in the ideal stoichiometry, produced a blue microcrystalline powder with a color matching that of bulk Cu<sub>3</sub>(BTC)<sub>2</sub>. Samples with an excess of metal ions present (1:2, 1:3) produced similarly blue powders although a greater degree of cracking was observed after drying. SEM images (ESI Figure S3, Supporting Information) further illustrate the cracks in the printed MOF. For ratios where an excess of the H<sub>3</sub>BTC ligand was present (1:1, 2:1, 3:1, and 3:2), large needle-like crystals matching those obtained by printing H<sub>3</sub>BTC alone were

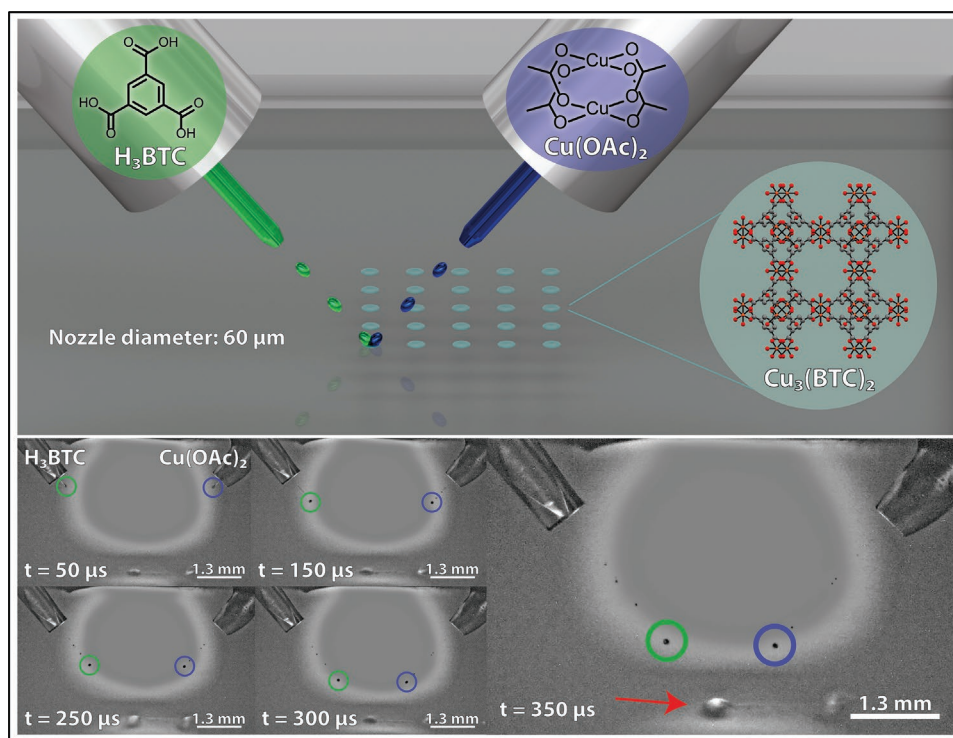


**Figure 1.** (Top) Schematic representation of the printing process of a  $5 \times 5$  dot array: Green droplets and the left jetting nozzle ( $60 \mu\text{m}$  nozzle diameter) represent Ligand Ink A ( $\text{H}_3\text{BTC}$   $0.25 \text{ m}$  in DMF), chemical structure shown above (right); blue droplets and the right jetting nozzle ( $60 \mu\text{m}$  nozzle diameter) depict metal ink B ( $\text{Cu}(\text{OAc})_2$   $0.25 \text{ m}$  in DMF), chemical structure shown above (left). (Right top inset) Ball and stick representation of the synthesized  $\text{Cu}_3(\text{BTC})_2$  MOF structure schematically depicted by the turquoise dot array. (Bottom) Strobe time lapse images of droplet formation of DMF solutions of  $\text{H}_3\text{BTC}$  (green) and  $\text{Cu}(\text{OAc})_2$  (blue)  $60 \mu\text{m}$  nozzle diameters microFab jetting devices during printing of MOF lines (red arrow) on coverglass substrates with a custom built printer platform.

observed. This was attributed to the relatively low solubility of  $\text{H}_3\text{BTC}$  in DMF, compared to  $\text{Cu}(\text{OAc})_2$ , which would result in the nucleation of  $\text{H}_3\text{BTC}$  crystals before the  $\text{H}_3\text{BTC}$  could react with  $\text{Cu}(\text{OAc})_2$  to form  $\text{Cu}_3(\text{BTC})_2$ .

Raman spectroscopy was used to screen the droplets for  $\text{Cu}_3(\text{BTC})_2$  formation. Two new peaks were observed at  $500$  and  $820 \text{ cm}^{-1}$ , corresponding to bulk MOF produced via conventional synthesis, which confirmed the successful formation of the target MOF (Figure 2A).<sup>[37]</sup> The presence of these two peaks were observed most strongly in the 2:3 and 1:3 (shown in Figure 2A) ratio samples, as well as the 1:2 sample; they were also observed to a lesser extent in the 3:2 and 3:1 ratio samples, when an excess of ligand was present. The formation of  $\text{Cu}_3(\text{BTC})_2$  was confirmed by printing dot arrays onto zero background silicon wafers (Si100) in the 2:3 and 1:3 ratios and analyzing them using X-ray powder diffraction (XRPD) (Figure 2B). The diffraction patterns for the printed materials closely match with those of the calculated patterns for  $\text{Cu}_3(\text{BTC})_2$  and that of bulk material synthesized by repeating a previously reported hydrothermal synthesis.<sup>[37]</sup>

## 2.2. RIJ of a Multivariate MOF Gradient

A key advantage of MOFs is that they have a modular structure which allows for mixing and matching of different combinations of ligands and metal ions without changing the

underlying structure of the MOFs. This concept of “isoreticular substitution” has been used to create diverse libraries of different frameworks with different functionalities.<sup>[38]</sup> It has also enabled the creation of “multivariate” frameworks (MTV-MOFs) which blend two or more different ligands or metal ions within a single framework with the same structure.<sup>[39]</sup> Applying these principles to RIJ opens up the possibility of using the same precursor inks to print different MOFs and using spatial control to enable the printing of gradients that transition from one structure to another via a multivariate phase. To our knowledge, no previous examples of such MTV-MOF gradients have been printed.

Six inks were prepared as DMF solutions of acetate salts of Cu, Zn and Co as well as ligands  $\text{H}_2\text{BDC}$  (1,4-benzene dicarboxylic acid),  $\text{H}_2\text{ABDC}$  (2-amino-1,4-benzene dicarboxylic acid) and HBIM (benzimidazole). The relevant inks were then combined through RIJ at ratios of 1:1 droplets, where the ink concentrations were  $0.25 \text{ m}$  for all inks except BIM which was  $0.5 \text{ m}$  to preserve the correct stoichiometry. These were used to print (Figure 2C) four well-known previously reported MOFs:  $\text{Cu}(\text{BDC})$ ,<sup>[40]</sup>  $\text{Cu}(\text{ABDC})$ ,<sup>[41]</sup>  $\text{Zn}(\text{BIM})_2$  and  $\text{Co}(\text{BIM})_2$ .<sup>[42]</sup> The structure of each printed MOF was then analyzed by XRPD (Figure 2D; Figure S8, Supporting Information) and Raman analysis (ESI Figure S7,S9, Supporting Information) and compared to patterns generated from known crystal structures and material made via previously reported bulk synthesis, confirming the formation of the expected structures.



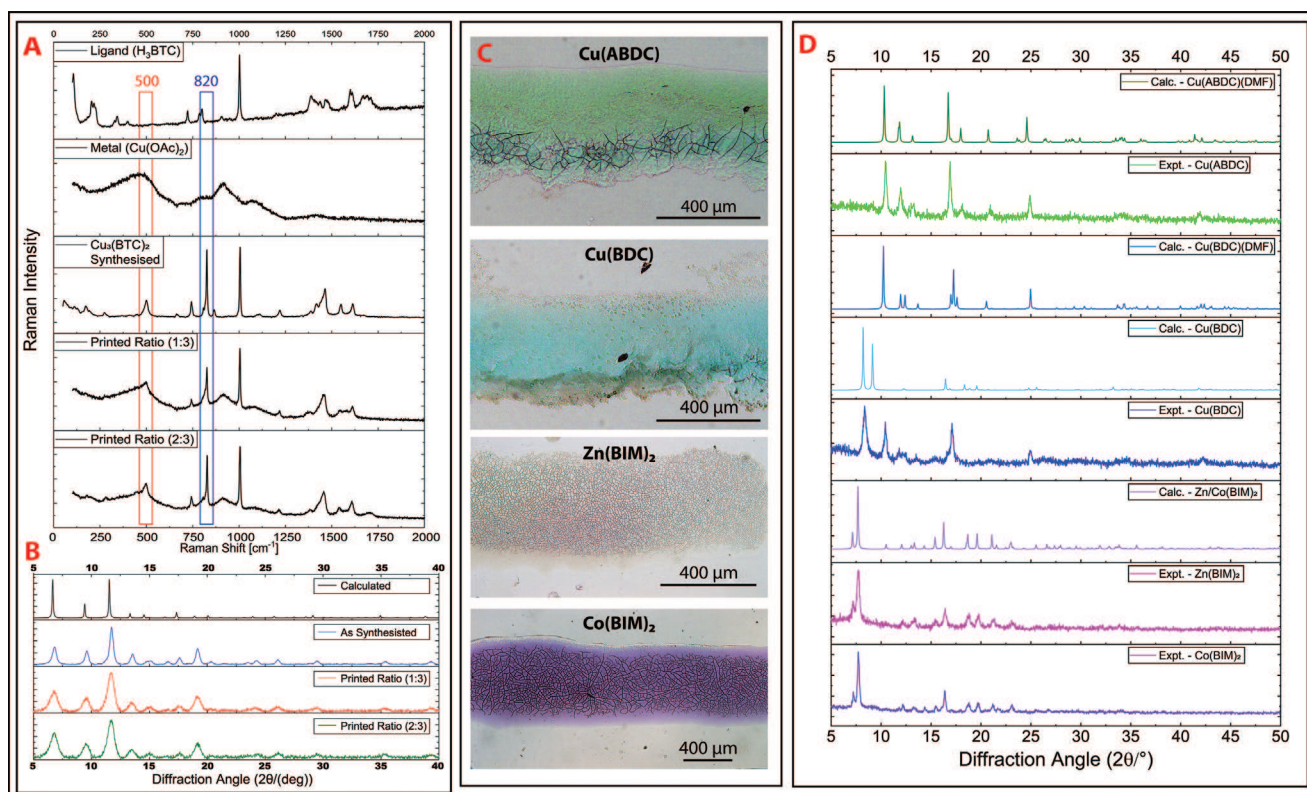


**Figure 2.** A) Raman spectroscopy of the ligand ( $\text{H}_3\text{BTC}$ ) and metal ( $\text{Cu}(\text{OAc})_2$ ) reagents, the bulk synthesized MOF (for comparison) and the two RIJ samples at ratios of 2:3 and 1:3. The two RIJ samples exhibit peaks at  $500$  and  $820\text{ cm}^{-1}$ , which confirms successful synthesis. B) XRPD patterns for the calculated MOF, bulk MOF and the two RIJ samples, showing that the target peaks for the MOF are present in the two RIJ samples. C) Optical micrographs of printed lines of the other MOFs produced by RIJ exhibiting the different colors that are due to the different synthesized MOF species. D) XRPD patterns comparing phase of printed MOFs to bulk and literature examples, which demonstrate successful synthesis of the MOFs.

As shown in **Figure 3A**, by keeping the amount of Cu ink constant but varying the ratio of BDC to ABDC linker, a gradient from 100%  $\text{Cu}(\text{BDC})$  to 100%  $\text{Cu}(\text{ABDC})$  was achieved. This gradient was observed visually; the line changes from blue to green. XRPD of samples prepared at different ratios confirm the formation of MTV MOFs, with samples up to 50% loading of BDC showing only peaks matching the  $\text{Cu}(\text{ABDC})(\text{DMF})$  structure (Figure S6, Supporting Information). At 50% loading of BDC and above, additional peaks are observed which correspond to blends which correspond to the desolvated form of  $\text{Cu}(\text{BDC})$ .<sup>[40,43]</sup> Raman microscopy was used to record spectra along the printed line (indicated by 1 to 5 Figure 3A) which showed the gradual loss of bands associated with the BDC MOF along with the gradual growth of broader bands characteristic of the ABDC MOF. The broadness of the  $\text{Cu}(\text{ABDC})$  Raman bands were attributed to the smaller size of the crystallites obtained due to rapid crystal growth by the more basic ABDC linker.

A gradient of metal ions was produced in a similar way by varying the ratio of Zn and Co inks added to the BIM ink as shown in ESI Figure S5 (Supporting Information). Raman analysis shows no significant changes along the printed gradient line consistent with Raman inactive metal ions forming a consistent structure (ESI Figure S8,S9, Supporting Information). However, a clear change in color from purple to white can be observed. Some breaking of the printed lines is observed as the

system was less well optimized to the different growth kinetics of these systems (ESI Figure S5, Supporting Information).

As detailed in the experimental section, in these examples gradient printing was achieved by pre-mixing components within the inks as limitations of the equipment available meant only two inks could be printed at a time. However, an upgraded system with three nozzles could achieve a more refined effect by altering the number of droplets of each ink added through a similar process used to optimize the ratio of  $\text{Cu}_3(\text{BTC})_2$ .

### 2.3. Selective Adsorption of Dyes by Printed Framework

As a step toward lab-on-a-chip type applications, we investigated whether printed MOFs could be used to selectively encapsulate dyes. Two dyes, Methylene Blue ( $\lambda_{\text{ex}}$  662–666 nm,  $\lambda_{\text{em}}$  686 nm) and Rhodamine B ( $\lambda_{\text{ex}}$  542–554 nm,  $\lambda_{\text{em}}$  567 nm) were investigated as these have sizes greater, and less than, the aperture sizes of  $\text{Cu}_3(\text{BTC})_2$  (10 and 14 Å). We hypothesized that methylene blue would be encapsulated inside the MOF whilst Rhodamine B would not. This size selectivity has been previously demonstrated for  $\text{Cu}_3(\text{BTC})_2$  grown in nano-confined fluidic channels.<sup>[44]</sup>

Lines of  $\text{Cu}_3(\text{BTC})_2$  (10 mm long) were printed onto glass substrates at 1:3 and 2:3 ratios (Figure 3; ESI Figure S11, Supporting Information). They were then immersed for 24 h in

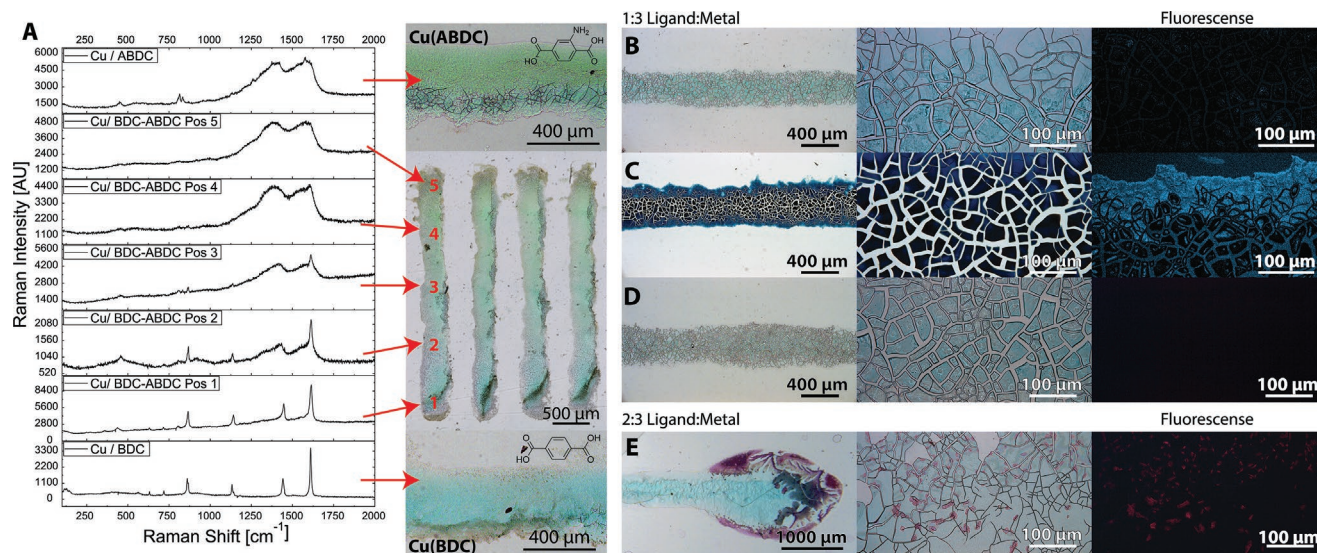


**Figure 3.** A) Raman spectra and optical micrographs showing gradient printing of multivariate Cu(ABDC):Cu(BDC) MOFs taken at different positions. Optical microscope brightfield and fluorescence images of representative printed MOF lines on coverglass substrates with five times material printed at 1:3 B–D) and 2:3 E) ( $\text{H}_3\text{BTC} : \text{Cu}(\text{OAc})_2$  0.25 M in DMF): B) Before and after 24 h incubation in a solution of Methylene Blue in ethanol C) and Rhodamine B solution in Ethanol) D and E), which shows incorporation of the smaller methylene blue dye, but not the larger rhodamine dye within the pores of the MOF.

solutions of ethanol saturated with either Methylene Blue or Rhodamine B. The samples were removed from the dye solution and carefully rinsed with fresh ethanol. With a 2:3 ratio rhodamine B was found to stick to needle-like crystals which was attributed to electrostatic interactions between the positively charged dye and excess BTC ligands. However, for the 1:3 ratio, lines of MOF immersed in methylene blue (Figure 3E) show a deep blue color under bright-field illumination and blue fluorescence in the dark field images. In contrast, no distinctive red stains and no visible fluorescence was observed following immersion in the Rhodamine B dye solution (Figure 3D). These observations indicate that as expected, the smaller Methylene blue dye molecules are absorbed within the pores of the framework whilst the larger Rhodamine B dye molecules are washed off.

### 3. Conclusions

Here, we demonstrate RIJ as a new approach to the patterning of surfaces with MOFs which allows control over the composition as well as position of the printed material. We used a custom built inkjet printer fitted with an angled jetting device to simultaneously print picolitre quantities of separate solutions of metal ions and ligands onto a surface which reacted at room temperature to form a MOF. The use of separate solutions of metal-ions and organic ligands avoids issues associated with the use of conventional inkjet printing approaches where pre-formed particles can lead to clogging of print-heads and extensive washing/drying procedures are needed to remove stabilizing agents. As with other inkjet printing methods, the MOFs could be printed into a variety of different complex shapes demonstrating spatial control. The versatility of the approach was shown by printing five

different MOFs:  $\text{Cu}_3(\text{BTC})_2$ , Cu(BDC), Cu(ABDC),  $\text{Zn}(\text{BIM})_2$ , and  $\text{Co}(\text{BIM})_2$ . The porosity of the printed  $\text{Cu}_3(\text{BTC})_2$  was confirmed and utilized through size-selective absorption of a fluorescent dye demonstrating one potential application of RIJ MOFs.

A key advantage of the RIJ approach over other printing techniques is that the composition of the printed material can readily be varied. MOFs are a uniquely interesting system to investigate in this regard because their modular structure means different solutions of ligands and metal-ions can be brought together in a “mix-and-match” way to tune the composition of the MOFs. We demonstrate this by showing how printing different ratios of components allowed the stoichiometry of  $\text{Cu}_3(\text{BTC})_2$  to be optimized removing the need for washing steps. A slight excess of metal-ions was found to be optimal for the printing of  $\text{Cu}_3(\text{BTC})_2$  MOF formation and prevent the formation of needle-like ligand crystals during the printing of  $\text{Cu}_3(\text{BTC})_2$ . Uniquely, this approach also enabled the printing of a MOF gradient in which the composition of components within an isoreticular series of MOFs gradually varies. Lines were printed in which the percentage of ligand gradually varied from 100% BDC to 100% ABDC and metal ions changed from Zn to Co without changing the underlying MOF structure. To our knowledge, this type of gradient has not been achieved using any other patterning approaches and offers exciting opportunities for creating advanced coatings and devices where properties change gradually across a surface.

The ability to process MOFs into complex shapes and patterns is key to harnessing their diverse properties for use in real world devices. The ability to mix-and-match stable solutions of components to print different structures, optimize their composition and print gradients are key advantages of RIJ over other patterning techniques. We anticipate that this approach will be broadly applicable to a wide range of other



MOFs and related materials enabling them to be blended together in increasingly sophisticated ways to create advanced coatings and devices.

## Supporting Information

Supporting Information is available from the Wiley Online Library or from the author.

## Acknowledgements

The authors thank the Royal Society (RG170002) and the Engineering and Physical Research Council (EP/L016281/1) for funding. The authors thank Dr Nicola Green for help with Confocal Imaging, Dr Xiubo Zhao for access to lab equipment and Christopher Hill for SEM analysis.

## Conflict of Interest

The authors declare no conflict of interest.

## Author Contributions

Printer development and printing and characterization along with drafting of the manuscript was primarily undertaken by D.A.G. J.N. undertook MOF synthesis and characterization and edited the manuscript. J.A.A. undertook preliminary printing and MOF studies and concept development. MSH undertook SEM and AFM characterization. J.A.F. and P.S. helped with conceptualization, analysis, resources, and reviewing and editing of the manuscript.

## Data Availability Statement

The data that support the findings of this study are available in the Supporting Information of this article.

## Keywords

metal–organic frameworks, micro-patterning, reactive inkjet printing, sensing devices, supramolecular chemistry

Received: January 17, 2023  
Published online:

- [1] J. Nicks, K. Sasitharan, R. R. Prasad, D. J. Ashworth, J. A. Foster, *Adv. Funct. Mater.* **2021**, *31*, 2103723.  
[2] Q. Qian, P. A. Asinger, M. J. Lee, G. Han, K. Mizrahi Rodriguez, S. Lin, F. M. Benedetti, A. X. Wu, W. S. Chi, Z. P. Smith, *Chem. Rev.* **2020**, *120*, 8161.  
[3] A. Bavykina, N. Kolobov, I. S. Khan, J. A. Bau, A. Ramirez, J. Gascon, *Chem. Rev.* **2020**, *120*, 8468.  
[4] L. E. Kreno, K. Leong, O. K. Farha, M. Allendorf, R. P. Van Duyne, J. T. Hupp, *Chem. Rev.* **2012**, *112*, 1105.  
[5] E. M. Dias, C. Petit, *J. Mater. Chem. A* **2015**, *3*, 22484.  
[6] L. Wang, M. Zheng, Z. Xie, *J. Mater. Chem. B* **2018**, *6*, 707.  
[7] V. Stavila, A. A. Talin, M. D. Allendorf, *Chem. Soc. Rev.* **2014**, *43*, 5994.

- [8] P. Falcaro, D. Buso, A. J. Hill, C. M. Doherty, *Adv. Mater.* **2012**, *24*, 3153.  
[9] O. Shekhan, J. Liu, R. A. Fischer, C. Woll, *Chem. Soc. Rev.* **2011**, *40*, 1081.  
[10] B. Hoppe, K. D. J. Hindricks, D. P. Warwas, H. A. Schulze, A. Mohmeyer, T. J. Pinkvos, S. Zailskas, M. R. Krey, C. Belke, S. König, M. Fröba, R. J. Haug, P. Behrens, *CrystEngComm* **2018**, *20*, 6458.  
[11] Y. Huang, C. A. Tao, R. Chen, L. Sheng, J. Wang, *Nanomaterials* **2018**, *8*.  
[12] L. Sarango, L. Pasetta, M. Navarro, B. Zornoza, J. Coronas, *J. Ind. Eng. Chem.* **2018**, *59*, 8.  
[13] a) O. Dalstein, D. R. Ceratti, C. Boissière, D. Grosso, A. Cattoni, M. Faustini, *Adv. Funct. Mater.* **2016**, *26*, 81; b) G. Lu, O. K. Farha, W. Zhang, F. Huo, J. T. Hupp, *Adv. Mater.* **2012**, *24*, 3970.  
[14] D. Witters, N. Vergauwe, R. Ameloot, S. Vermeir, D. De Vos, R. Puers, B. Sels, J. Lammertyn, *Adv. Mater.* **2012**, *24*, 1316.  
[15] a) I. D. Williams, *Nat. Chem.* **2014**, *6*, 953; b) H. Thakkar, S. Eastman, Q. Al-Naddaf, A. A. Rowan, F. Rezaei, *ACS Appl. Mater. Interfaces* **2017**, *9*, 35908; c) G. J. H. Lim, Y. Wu, B. B. Shah, J. J. Koh, C. K. Liu, D. Zhao, A. K. Cheetham, J. Wang, J. Ding, *ACS Mater. Lett.* **2019**, *1*, 147.  
[16] a) R. Zhao, Y. Tian, S. Li, T. Ma, H. Lei, G. Zhu, *J. Mater. Chem. A* **2019**, *7*, 22559; b) C.-L. Zhang, B.-R. Lu, F.-H. Cao, Z.-Y. Wu, W. Zhang, H.-P. Cong, S.-H. Yu, *Nano Energy* **2019**, *55*, 226.  
[17] a) J. Hou, A. F. Sapnik, T. D. Bennett, *Chem. Sci.* **2020**, *11*, 310; b) A. Carné-Sánchez, I. Imaz, M. Cano-Sarabia, D. MasPOCH, *Nat. Chem.* **2013**, *5*, 203.  
[18] a) P. J. Smith, A. Morrin, *J. Mater. Chem.* **2012**, *22*, 10965; b) Y. Yoshioka, G. E. Jabbour, *Synth. Met.* **2006**, *156*, 779.  
[19] a) R. A. Street, W. S. Wong, S. E. Ready, M. L. Chabinyk, A. C. Arias, S. Limb, A. Salleo, R. Lujan, *Mater. Today* **2006**, *9*, 32; b) A. C. , M. Z. Szymanski, B. Luszczynska, J. Ulanski, *Sci. Rep.* **2019**, *9*, 8493.  
[20] a) S. K. Karunakaran, G. M. Arumugam, W. Yang, S. Ge, S. N. Khan, X. Lin, G. Yang, *J. Mater. Chem. A* **2019**, *7*, 13873; b) S. Sumaiya, K. Kardel, A. El-Shahat, *Technologies* **2017**, *5*.  
[21] H. Maleki, V. Bertola, *Catal. Sci. Technol.* **2020**, *10*, 3140.  
[22] a) J. R. Verkouteren, J. Lawrence, T. M. Brewer, E. Sisco, *Anal. Methods* **2017**, *9*, 3441; b) J. Wang, L. Yang, B. Liu, H. Jiang, R. Liu, J. Yang, G. Han, Q. Mei, Z. Zhang, *Anal. Chem.* **2014**, *86*, 3338.  
[23] a) P. M. Grubb, H. Subbaraman, S. Park, D. Akinwande, R. T. Chen, *Sci. Rep.* **2017**, *7*, 1202; b) S. Chung, K. Cho, T. Lee, *Adv. Sci.* **2019**, *6*, 1801445.  
[24] B. Huber, P. B. Popp, M. Kaiser, A. Ruediger, C. Schindler, *Appl. Phys. Lett.* **2017**, *110*.  
[25] T.-T. Huang, W. Wu, *J. Mater. Chem. A* **2019**, *7*, 23280.  
[26] a) D. A. Gregory, P. Kumar, A. Jimenez-Franco, Y. Zhang, Y. Zhang, S. J. Ebbens, X. Zhao, *J. Vis. Exp.* **2019**, <https://doi.org/10.3791/59030e59030>; b) Y. Zhang, D. A. Gregory, Y. Zhang, P. J. Smith, S. J. Ebbens, X. Zhao, *Small* **2018**, *15*, 1804213; c) D. A. Gregory, Y. Zhang, P. J. Smith, S. J. Ebbens, X. Zhao, *Small* **2016**, *12*, 4048.  
[27] a) R. D. Boehm, P. R. Miller, J. Daniels, S. Stafslin, R. J. Narayan, *Mater. Today* **2014**, *17*, 247; b) N. Scoutaris, S. Ross, D. Douroumis, *Pharm. Res.* **2016**, *33*, 1799.  
[28] P. Goel, S. Singh, H. Kaur, S. Mishra, A. Deep, *Sens. Actuators, B* **2021**, *329*, 129157.  
[29] L. L. Da Luz, R. Milani, J. F. Felix, I. R. B. Ribeiro, M. Talhavini, B. A. D. Neto, J. Chojnacki, M. O. Rodrigues, S. A. Júnior, *ACS Appl. Mater. Interfaces* **2015**, *7*, 27115.  
[30] C. Zhang, B. Wang, W. Li, S. Huang, L. Kong, Z. Li, L. Li, *Nat. Commun.* **2017**, *8*.  
[31] C.-H. Su, C.-W. Kung, T.-H. Chang, H.-C. Lu, K.-C. Ho, Y.-C. Liao, *J. Mater. Chem.* **2016**, *4*, 11094.

- [32] J. L. Zhuang, D. Ar, X. J. Yu, J. X. Liu, A. Terfort, *Adv. Mater.* **2013**, 25, 4631.
- [33] M. Hou, H. Zhao, Y. Feng, J. Ge, *Bioresour Bioprocess* **2017**, 4.
- [34] A. J. Lennon, A. WY Ho-Baillie, S. R Wenham, *Sol. Energy Mater. Sol. Cells* **2009**, 93, 1865.
- [35] F. Al-Ghazzawi, L. Conte, C. Richardson, P. Wagner, *Angew. Chem., Int. Ed.* **2022**, 61.
- [36] a) R. Ameloot, E. Gobechiya, H. Uji-i, J. A. Martens, J. Hofkens, L. Alaerts, B. F. Sels, D. E. De Vos, *Adv. Mater.* **2010**, 22, 2685; b) J. L. Zhuang, D. Ceglarek, S. Pethuraj, A. Terfort, *Adv. Funct. Mater.* **2011**, 21, 1442; c) T. Wang, H. Zhu, Q. Zeng, D. Liu, *Adv. Mater. Interfaces* **2019**, 6.
- [37] S. S. Chui, S. M. Lo, J. P. Charmant, A. G. Orpen, I. D. Williams, *Science* **1999**, 283, 1148.
- [38] M. Eddaoudi, J. Kim, N. Rosi, D. Vodak, J. Wachter, M. O’Keeffe, O. M. Yaghi, *Science* **2002**, 295, 469.
- [39] a) H. Deng, C. J. Doonan, H. Furukawa, R. B. Ferreira, J. Towne, C. B. Knobler, B. Wang, O. M. Yaghi, *Science* **2010**, 327, 846; b) D. J. Ashworth, J. A. Foster, *Nanoscale* **2020**, 12, 7986.
- [40] C. G. Carson, K. Hardcastle, J. Schwartz, X. Liu, C. Hoffmann, R. A. Gerhardt, R. Tannenbaum, *Eur. J. Inorg. Chem.* **2009**, 2009, 2338.
- [41] J. Nicks, J. Zhang, J. A. Foster, *Chem. Commun.* **2019**, 55, 8788.
- [42] K. S. Park, Z. Ni, A. P. Cote, J. Y. Choi, R. Huang, F. J. Uribe-Romo, H. K. Chae, M. O’Keeffe, O. M. Yaghi, *Proceedings of the National Academy of Science U. S. A.* **2006**, 103, 10186.
- [43] C. G. Carson, G. Brunello, S. G. Lee, S. S. Jang, R. A. Gerhardt, R. Tannenbaum, *Eur. J. Inorg. Chem.* **2014**, 2014, 2140.
- [44] S. Guthrie, L. Huelsenbeck, A. Salahi, W. Varhue, N. Smith, X. Yu, L. U. Yoon, J. J. Choi, N. Swami, G. Giri, *Nanoscale Adv* **2019**, 1, 2946.